Time–time-transform-based fault location algorithm for three-terminal transmission lines

Alireza Ahmadimanesh, Seyyed Mohammad Shahrtash

Center of Excellence for Power Systems Automation and Operation, Iran University of Science and Technology, Narmak, Tehran, Iran
E-mail: shahrtash@iust.ac.ir

Abstract: In this study, time–time transformation is employed to reveal the time of arrival of the fault-generated travelling waves, where these time instants are then used in a fault location algorithm for three-terminal single- and double-circuit transmission lines. The performance of the proposed fault location algorithm under different line lengths and fault conditions such as fault types, faulted sections, fault locations, fault resistances and fault inception angles are investigated and the high accuracy of the proposed method is approved in all these conditions even, in fault inception angle of zero and for faults on tap point.

1 Introduction

Fault location is one of the important tasks for power system utilities. Different methods have been presented to provide this information from the measured voltage and current data at the terminals of a transmission line. These methods can be classified into three categories: impedance-based, artificial intelligence-based and transient-based methods [1]. In another point of view, these methods can be classified as those which need the data from all terminals (either synchronised or non-synchronised) and those which only use the data from the local terminal [1].

Narrowing the extent of literature survey to transient-based methods employed in fault location task, generally, these methods take advantages of the high-frequency components of voltage or current initiated by faults. Thus, there are two problems associated with them, that is,

- need to high sampling frequency, f_s, to be able in revealing high-frequency components of a signal, and
- difficulty in detecting faults with zero fault inception angle, where the fault initiated transients are very low.

Despite to these facts, there are various papers in this area with two approaches, including inspection of fault initiated transients and circuit breaker opening transients. From the first approach, the method in [2] is based on travelling waves and it uses a characteristic method (i.e. directly processing the receiving waves) to find the fault location (with $f_s = 500$ kHz). Alternatively, Wavelet transform has been applied for revealing the arrival time of the waves to the terminals, in fault location procedure [3–7]. In [3], first the faulted segment (first or second half of line) is selected by using the difference in arrival time of modal components, and then the fault location is calculated (with $f_s = 333$ kHz). In [4], by improving the method of [3],

applied for two-terminal transmission line, the combined effect of the sampling rate, the poor frequency response of transducers and the variation in reflection pattern that may give errors in results have been considered and an alternative method by employing polarity of the signal has been proposed . The analysis in this paper is based on recorded data sampled at 1.25 MHz. In [5, 6], by using a hybrid method that has used fundamental frequency component when high value noise exists and travelling wave method for lower noises, the fault location has been found (with $f_s = 240$ kHz). In [8], the differences between aerial and ground modes of current signal are used for fault location in two-terminal power transmission lines. Although in this algorithm the data from only one terminal is used for the fault location, the sampling frequency must be very high (almost 7 MHz) in order to have a good accuracy; whereas this method is only applicable to ground faults. Mathematical morphology has been used in [9] to extract the arrival time of wave from all terminals and then the fault location has been found (with $f_s = 1$ MHz). From the second approach, in [10], the proposed fault location methods have employed fault clearing transients (with $f_s = 40$ kHz). Although in these algorithms voltage signals are used and the errors because of current transformers are eliminated, the main problem in these methods is the non-simultaneous opening of circuit breakers in three phases which makes the estimation accuracy to be very low.

In this paper, a new fault location method, based on travelling waves initiated by faults, is presented for both single- and double-circuit three-terminal lines which does not need very high sampling rate. The main tool in the proposed scheme is TT-transform (stands for time–time transformation) which is applied for the purpose of calculating reliable indices from appropriate modes of the currents in three phases, in order to provide the fault detection function and to be used as an indication for

revealing the arrival time of the incoming waves at line terminals. These results are then used for assigning the faulted section and estimating the fault location with an acceptable accuracy and speed. The proposed algorithm can deliver the fault location with negligible error under different conditions such as fault location, fault type, fault resistance and fault inception angle. It should be mentioned that the proposed algorithm needs synchronised data window for current measurements at the three terminals of transmission line.

The rest of this paper is structured as follows. Section 2 has explained TT-transform. The proposed method for single-circuit lines is introduced in Section 3 for which in the next section, the simulation results have been shown. The effect of different parameters and also extension of the algorithm to double-circuit lines are discussed in Section 4. A qualitative comparison between the proposed method and the existent travelling wave-based methods are given in Section 5. In the final section, the conclusions are presented.

2 TT-transform

TT-transform is a two-dimensional (2D) time–time representation of a 1D time series which gives a local time view of a scaled window. It makes a good time-local property of the time series, providing localised frequency components for it. TT-transform has been derived as an inverse Fourier transform of the time–frequency-transform and up to date only its diagonal elements have been used for signal characterisation [11]. These diagonal elements are defined as

$$TT(t, t) = F^{-1}\{U(f)G(f)\} \tag{1}$$

where F represents the Fourier transform, F^{-1} is its inverse,

U is the Fourier transform of the considered signal u, and G is defined by

$$G(f) = -2p_k \pi^2 |f| \tag{2}$$

where p_k is constant and for example $p_1 = -0.02199$, $p_3 = -0.00679$ and $p_5 = -0.00405$ [11]. In this paper, p_1 is only used for obtaining TT-transform.

The above relation is a modified definition for diagonal elements of TT-transform, proposed by Simon et al. [11]. The advantages of this form of TT-transform against its general form, introduced in [12], are its simplicity to be applied, having less computation burden and no need to $N \times N$ matrix, where the latter one is much more important especially when TT-transform is going to be implemented as a part of a control or protection algorithm in some power system transients software packages (such as EMTP).

The TT-transform has some features that make it different from the other feature extraction methods. The most important property of this transformation is that it is needless of choosing any function, such as mother wavelet in wavelet transform, and there is no need for selection of components at different levels, as its output has only one level. Another benefit of this transformation is in amplifying high-frequency components against low-frequency components. Therefore the high-frequency components, generated by the fault, can be detected much more easily.

For a typical fault in a three-terminal transmission line, the output of TT-transform on the mode-α of the current signal, in comparison with the travelling waves reached at the same terminal, are shown in Fig. 1. It can be seen that the peaks of the TT-transform of the current signal are good indicators for calculating the arrival time of corresponding waves to the terminals.
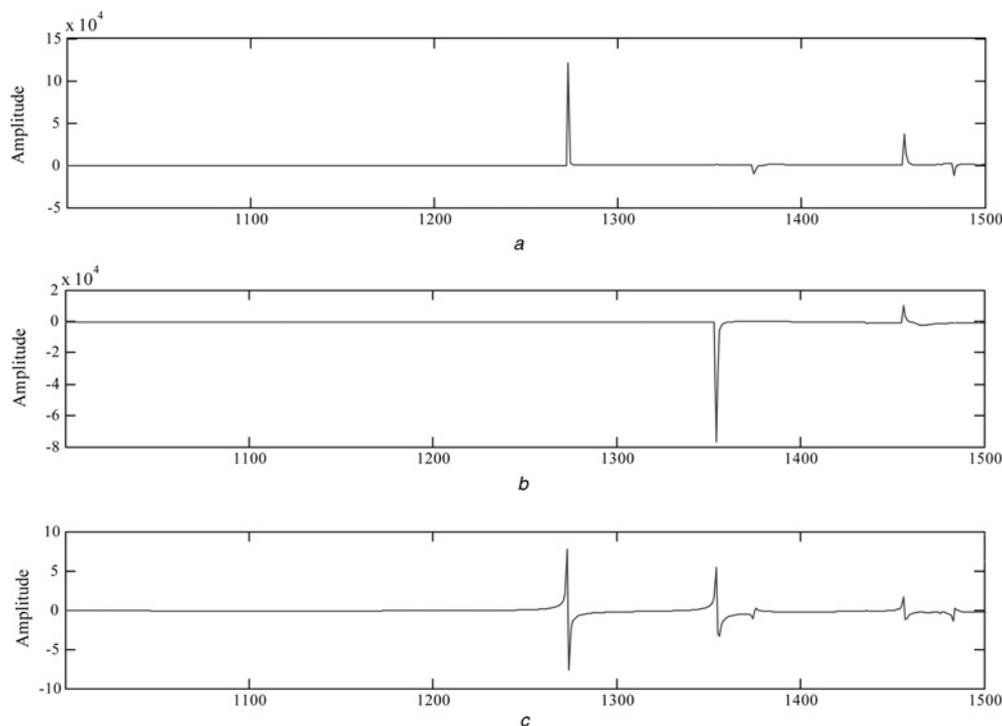

Fig. 1 *Performance of TT-transform upon fault generated transient components in current signal*
a Extracted backward current wave component
b Extracted forward current wave component
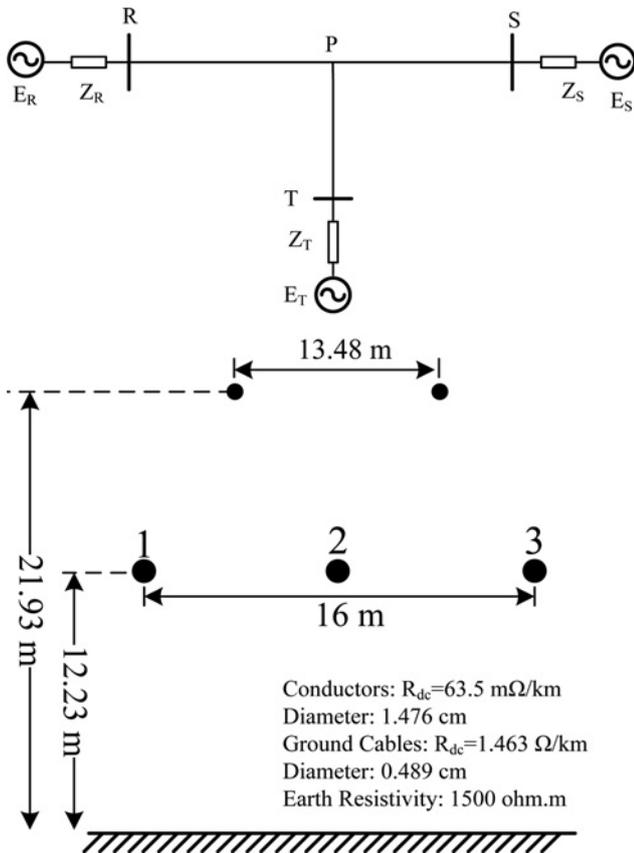c TT-transform output of corresponding current signal

Fig. 2 *Single-circuit three-terminal transmission line configuration*

Fig. 3 *Flowchart of the proposed scheme for fault location in three-terminal transmission lines*

3 Proposed fault location method

The proposed algorithm for fault location in single-circuit transmission line, shown in Fig. 2, is composed of two stages, including fault detection stage and fault location stage. The first stage, which needs only local data at each terminal, employs TT-transform to reveal the fault occurrence. The second stage, which should receive the time indices from all terminals, gives the estimation of fault location. The overall scheme of the proposed fault location algorithm is shown in Fig. 3 and its steps are explained in the following subsections.

3.1 Initialisations

The vital parameters that should be chosen before any further processing are as follows:

1. Sampling frequency (f_s)
2. Data window's length (DW)
3. Data window's moving step (DW_{step})

The first parameter is initially chosen as $f_s = 100$ kHz and the results with other values have been discussed in Section 4.6. In order to discriminate the waves initiated by the faults located at the minimum desired distance, L_{min}, the sampling frequency should be larger than (v/L_{min}), where v is the velocity of travelling waves in aerial modes. In other words, choosing a sampling rate, f_s, there arises a limitation on the minimum detectable location, which is (v/f_s).
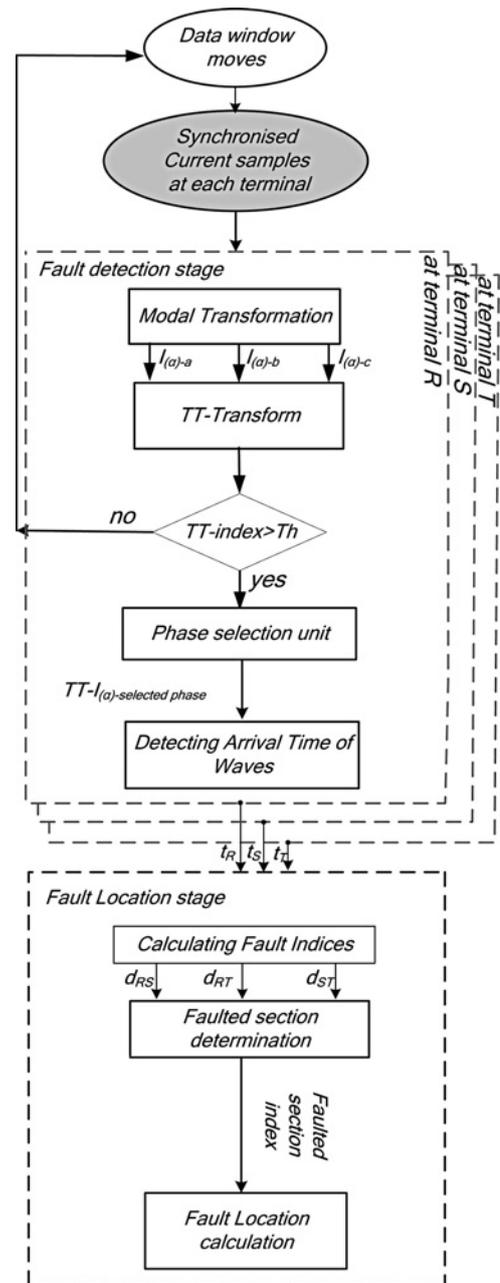
The second parameter, DW, should be greater than DW_{post} where the latter is defined by

$$DW_{post} \geq \frac{L_{max} \times f_s}{v} \qquad (3)$$

where L_{max} is the maximum length of line between two of the terminals.

The third parameter should be as much that the overlap between two subsequent data windows does not become less than DW_{post}; in order to preserve the coincidence of detection of waves at all terminals. In this work, to have the fastest speed in processing, the data window moves with the steps of

$$DW_{step} = DW - DW_{post} \qquad (4)$$

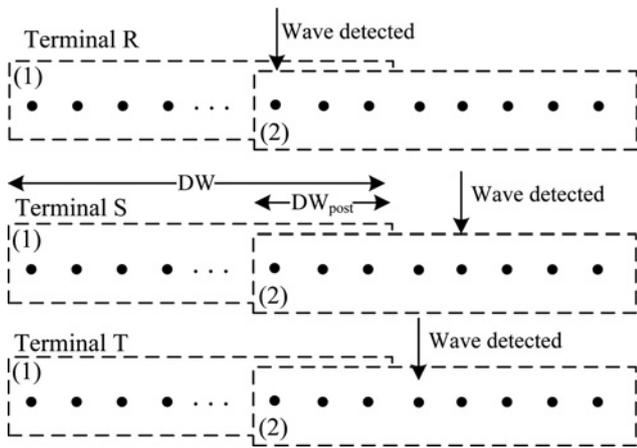In Fig. 4, the worst condition is shown; which is a fault near

Fig. 4 *Data window moving discipline and capturing receiving waves*

one of the terminals, detected in the sample number equal to $DW_{step} + 1$. Since this fault is far from the others, it has no contribution in the synchronised data window captured at the same time by the other two terminals. However, as data window moves, the fault is captured in the next data window at all three terminals, as shown in the same figure.

3.2 Fault detection stage

As shown in Fig. 3, this stage consists of five steps:

• First, modal transformation is applied to the samples of the current signal. For this purpose, the Clarke transformation is used

$$\left[I_{0\alpha\beta} \right] = \left[T_{Cl} \right] \cdot \left[I_{abc} \right] \tag{5}$$

where (for phase-a as the pivot)

$$T_{Cl} = \frac{1}{\sqrt{3}} \begin{bmatrix} 1 & 1 & 1 \\ \sqrt{2} & -\frac{1}{\sqrt{2}} & -\frac{1}{\sqrt{2}} \\ 0 & \frac{\sqrt{3}}{\sqrt{2}} & -\frac{\sqrt{3}}{\sqrt{2}} \end{bmatrix} \tag{6}$$

Similar transformations are made to find I_α for the other phases as pivots.

• In the second step, TT-transform is applied to the first aerial mode (I_α) of each phase, in order to detect the fault occurrence.
• By applying this transformation to all terminals' currents and comparing the numerical derivative of the TT-transform with a pre-defined threshold, the fault can be detected. In order to raise the robustness of the detector, this criterion should be fulfilled at three consequent samples. By inspection of this criterion at different terminals of the line and as soon as fault is detected at all terminals, the algorithm moves towards the fault location stage at all terminals.
• Then, phase selection unit selects the phase(s) with the largest output of TT-transform as the faulted phase(s).

• At the final step, by inspecting the TT-transform output (such as the one in Fig. 1), the time corresponding to the first peak is assigned as the time of arrival of the wave (e.g. t_R at terminal R in Fig. 2). The same procedures in the other two terminals result in t_S and t_T. As shown in Fig. 3, each terminal should receive this time index from the two other ones, as well, in order to proceed to the fault location stage.

3.3 Fault location stage

By receiving three time indices (one from local and two from the remote terminals), the fault location stage starts.

The steps of the fault location stage can be described as follows:

1. Finding faulted section: To find the faulted section, the fault location indices are calculated by the following equations

$$d_{RS} = \frac{l_{RS} - v(t_S - t_R)}{2} \tag{7}$$

$$d_{RT} = \frac{l_{RT} - v(t_T - t_R)}{2} \tag{8}$$

$$d_{ST} = \frac{l_{ST} - v(t_T - t_S)}{2} \tag{9}$$

where in these equations, t_i is the time associated with the first peak observed in the data window at each terminal (as shown in Fig. 5) and l_{ij} is the length between each two terminal. Then, to find the faulted line section (in Fig. 2), the following rules are employed [5]:

$d_{RT} \le l_{RP}$ and $d_{RS} \le l_{RP}$: the fault is on RP. Then d_{RT} or d_{RS} and/or their average can give the accurate fault location from R terminal.
$d_{RS} > l_{RP}$ and $d_{ST} < l_{SP}$: the fault is on SP. Then $(l_{RS} - d_{RS})$ or d_{ST} and/or their average can give the accurate fault location from S terminal.
$d_{RT} > l_{RP}$ and $d_{ST} \ge l_{SP}$: the fault is on TP. Then $(l_{RT} - d_{RT})$ or $(l_{ST} - d_{ST})$ and/or their average can give the accurate estimation of fault location from T terminal.

2. Fault location: According to the faulted section, found in the previous step, to provide the least estimation error, the corresponding indices are averaged to find the fault location, for example, if it is found that the faulted section is RP, then d_{RS} and d_{RT} will be averaged and assigned as d_{estim}.

Eventually, to have a quantitative index for evaluation of the proposed algorithm under different conditions, the estimation error is defined by

$$error(\%) = \frac{|d_{estim} - d_{exact}|}{L_{max}} \times 100 \tag{10}$$

where, L_{max} is previously defined.

4 Simulations and results

In order to verify the performance of the proposed fault location algorithm, the line shown in Fig. 2 (with the

system parameters given in the appendix) has been simulated under different fault conditions. In these simulations, frequency-dependent transmission line model has been used and all line sections have initially been assumed to be fully transposed.

Owing to the sampling frequency of 100 kHz and $L_{max} = 250$ km and according to (3), DW_{post} should contain at least 85 samples. Although this amount of samples are adequate, for better illustration of the results 120 samples have been considered for DW_{post}, whereas DW has been chosen as one fourth of fundamental frequency cycle.

Various conditions have been simulated by ATP/EMTP software and MATLAB has been used for analysing the current signals and calculating the fault location.

In these simulations, the influences of fault resistance, fault inception angle, fault type, external faults, lightning, unsynchronised data, pre-fault power flow, line lengths and also untransposed and double-circuit transmission lines have been investigated. Investigation on the contribution of each parameter has been done with the other parameters being kept as in the base case, unless it is mentioned.

4.1 Single-circuit case study

Fig. 5 has shown the output of applying TT-transform to the first aerial mode of the current signal (phase-a) at the three terminals. In this case study, fault is phase-a to ground with 30 Ω fault resistance and 30° fault inception angle at 30 km far from terminal R (in Fig. 2). As shown, the arrival times of waves have been detected as follows

$$t_R = 3.93 \, \text{ms}, \quad t_S = 4.57 \, \text{ms}, \quad t_T = 4.51 \, \text{ms}$$

Thus, according to (7)–(9), the fault location indices become

$$d_{RS} = 30.882 \, \text{km}, \quad d_{RT} = 29.706 \, \text{km}, \quad d_{ST} = 98.882 \, \text{km}$$

Refering to the rules employed in faulted section determination, as in this case, $d_{RS} < 150$ km and also $d_{RT} < 150$ km, the fault has occurred on RP section, and the fault location is $(d_{RT} + d_{RS})/2 = 30.29$ km far from R terminal, which according to (10) shows only 0.116% estimation error.
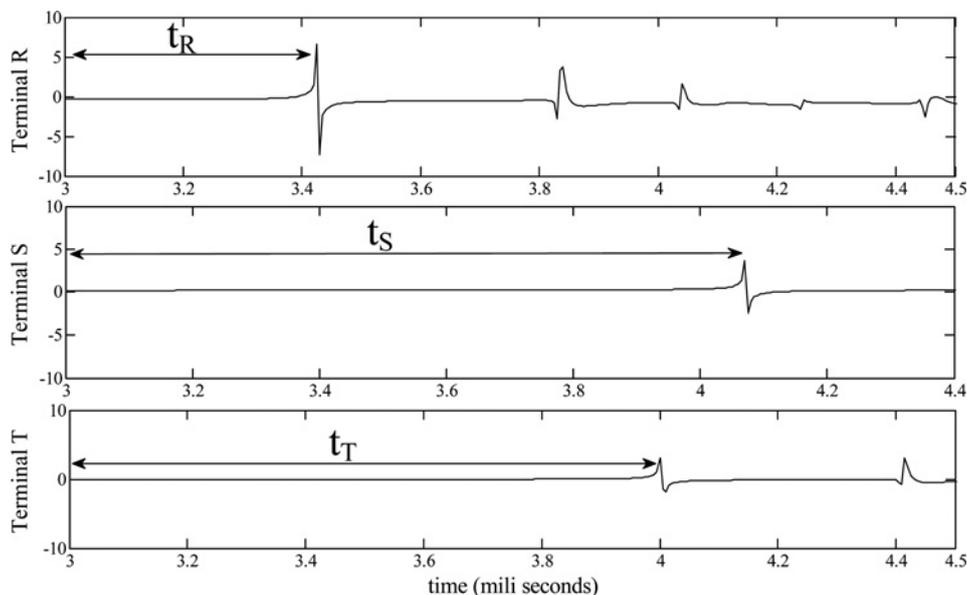

Fig. 5 *Outputs of applying TT-transform to aerial mode of current signals at the three terminals*

Table 1 Estimation error (in %) for different fault types, fault resistances and fault locations in single-circuit line

Fault type	Fault inception angle	Fault resistance, Ω	Fault location, km															
			10	20	30	40	50	60	70	75	80	90	100	110	120	130	140	Tap point
a–g	30°	1	0.18	0	0.18	0.24	0.06	0.18	0	0.06	0.18	0.06	0.06	0.41	0.29	0.18	0.06	0.13
a–g	30°	17	0.18	0	0.18	0.24	0.06	0.18	0	0.06	0.18	0.06	0.06	0.41	0.29	0.18	0.06	0.13
a–g	30°	50	0.18	0	0.18	0.24	0.06	0.18	0	0.06	0.18	0.06	0.06	0.41	0.29	0.18	0.06	0.13
a–g	30°	100	0.18	0	0.18	0.24	0.06	0.18	0	0.06	0.18	0.06	0.06	0.41	0.29	0.18	0.06	0.13
a–g	0°	30	0.47	0.29	0.12	0.53	0.06	0.12	0.29	0.24	0.18	0.24	0.06	0.12	0.29	0.18	0.35	0.14
b–c	30°	30	0.18	0.29	0.18	0.06	0.06	0.18	0.29	0.06	0.12	0.06	0.06	0.18	0.29	0.12	0.06	0.13
b–c–g	30°	30	0.18	0.29	0.18	0.06	0.06	0.18	0.29	0.06	0.12	0.06	0.06	0.18	0.29	0.12	0.06	0.13
a–b–c	30°	30	0.18	0.29	0.18	0.24	0.06	0.18	0.29	0.06	0.18	0.06	0.06	0.41	0.29	0.18	0.06	0.13
a–b–c–g	30°	30	0.18	0.29	0.18	0.24	0.06	0.18	0.29	0.06	0.18	0.06	0.06	0.41	0.29	0.18	0.06	0.13

4.2 Effect of fault location, fault resistance and fault type

Table 1 has shown the results of the proposed method for various fault locations on RP section (in Fig. 2) with different fault resistances under different fault types. As shown, the proposed method is not affected by fault type, fault resistance and fault location even when it has occurred on the tap point, where the errors in all conditions are under 0.5%.
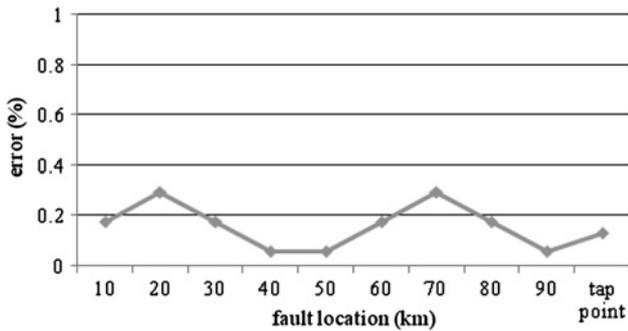

Fig. 6 *Estimation error for phase-a to ground fault at different locations on section TP (in Fig. 2)*

4.3 Effect of faulted section

To demonstrate the accuracy of the proposed algorithm in locating faults in different line sections, the results for faults located on different positions of TP section in Fig. 2, have been shown in Fig. 6 (the results of SP section is not
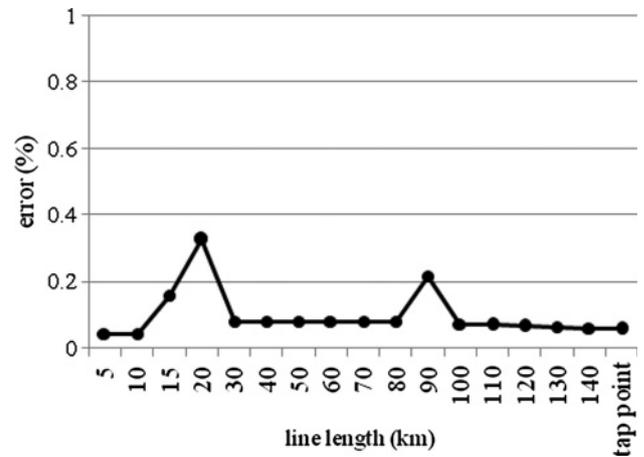

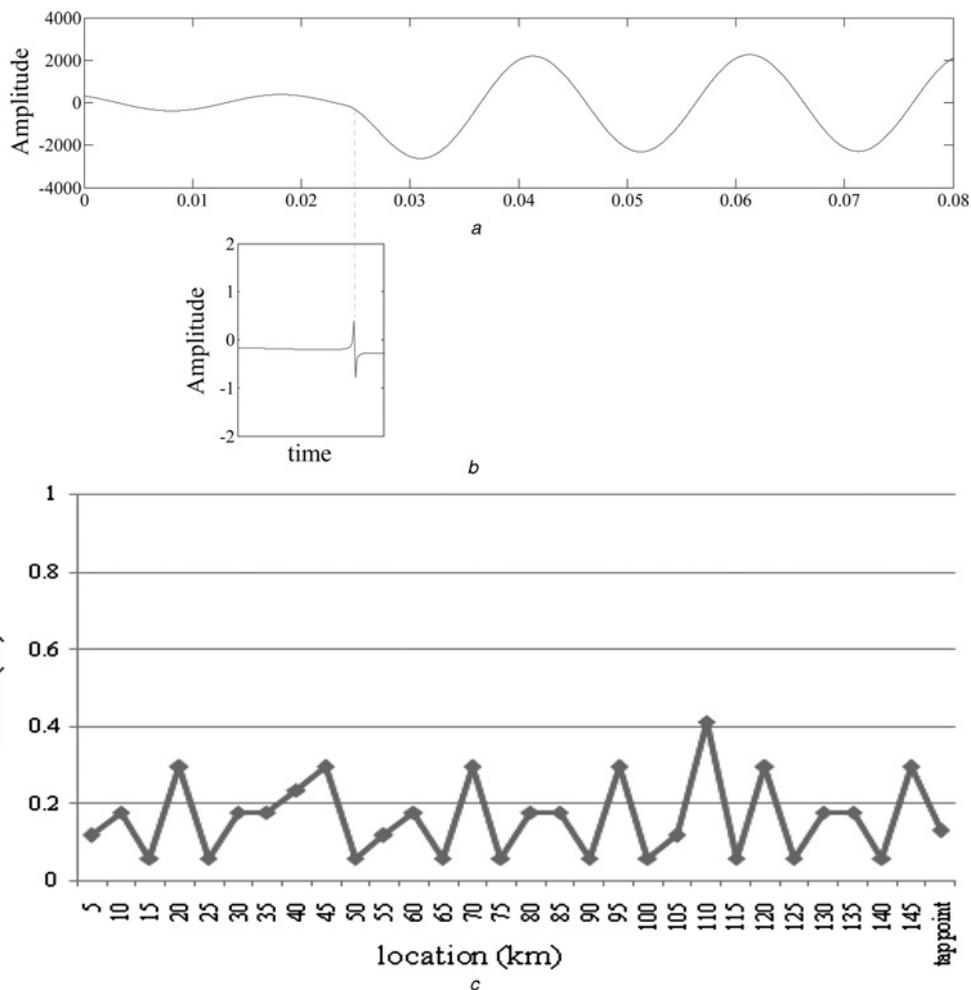**Fig. 7** *Estimation error for different line lengths*

Fig. 8 *Estimation error for faults with zero inception angle at different fault locations*
a Waveform of a current signal with fault occurred at zero inception angle
b Corresponding TT-transform
c Overall estimation error of the proposed method under this type of fault at different fault locations

Table 2 Estimation error (in %) for different sampling frequencies

Sampling frequency, kHz	Actual fault location, km																
	5	20	25	45	50	55	65	70	90	95	105	120	125	130	135	145	Tap point
50	0.53	0.64	0.29	0.54	0.28	0.51	0.2	0.56	0.37	0.02	0.11	0.59	0.24	0.12	0.48	0.6	0.6
76.92	0.5	0.15	0.15	0.21	0.29	0.38	0.18	0.26	0.15	0.32	0.26	0.38	0.09	0.18	0.5	0.06	0.13
100	0.12	0	0.06	0	0.06	0.12	0.06	0	0.06	0.29	0.12	0.29	0.06	0.18	0.18	0	0.13
200	0.03	0	0.06	0	0.06	0.03	0.06	0	0.06	0.15	0.03	0	0.06	0.03	0.18	0	0.093

shown to prevent lengthy paper). As shown, in all of them even on the tap point, faulted section is correctly found and the fault location algorithm performs as well as under the fault cases on the other line sections.

4.4 Effect of line length

Fig. 7 has shown the performance of the proposed method under different line length of RP section. In these simulations, the fault has been placed in the middle of RP section and as can be seen, the errors in all conditions are below 0.4%. These results have shown that the output of the proposed method is not affected by the length of transmission line even for short lines.

4.5 Effect of fault inception angles

The fault inception angle is one of the most effective parameters in the algorithms based on travelling waves. As shown in Fig. 8a, faults with zero inception angles have no substantial transients in the current waveform. Thus, many of the fault location methods that have employed the fault-generated transients cannot give a good response in these situations. However, owing to the features of TT-transform, that reveals any deformations in the waveform, as shown in Fig. 8b, the proposed fault location algorithm can estimate the fault location with high accuracy, even in these situations. The performance of the proposed fault location algorithm is shown in Fig. 8c, where keeping the fault inception angle at zero, the estimation error is shown for faults at different locations and for the tap point, as well.

4.6 Sampling frequency effect

Sampling frequency is another important parameter whose contribution on the performance of the proposed method

Table 3 Estimation error in untransposed lines

Fault location, km	Fault type	Fault resistance, Ω	Fault location error, %
30	ag	30	0.705
50	ag	30	0.352
120	ag	100	0.294
30	ag	100	0.705
tap point	ag	30	0.13
5	bc	50	0.176
75	bc	100	0.06
100	bcg	1	0.234
45	abc	30	0.294
145	abc	17	0.294
70	abcg	1	0

should be investigated. Generally, it is expected that higher sampling frequency gives higher accuracy in fault location estimation; because of the fact that the estimation error of the transient-based methods (especially those relying on time of arrival of travelling waves) is ideally relevant to $(c/2f_s)$, where c is the light velocity and f_s is the sampling frequency. This estimation error deviates from this ideal value for different algorithms and under various simulated fault conditions, but the mainstream of 'higher sampling frequency leads to higher accuracy' remains. Table 2 has shown the sampling frequency effect, for the fault along RP section (in Fig. 2) in zero fault inception angles, which approves the above statement.

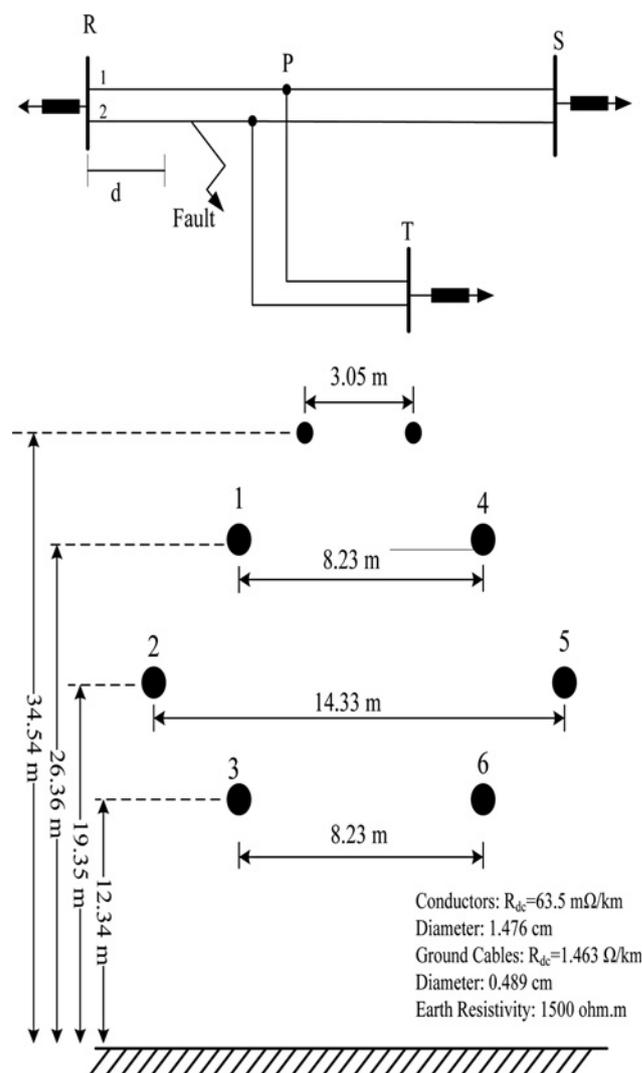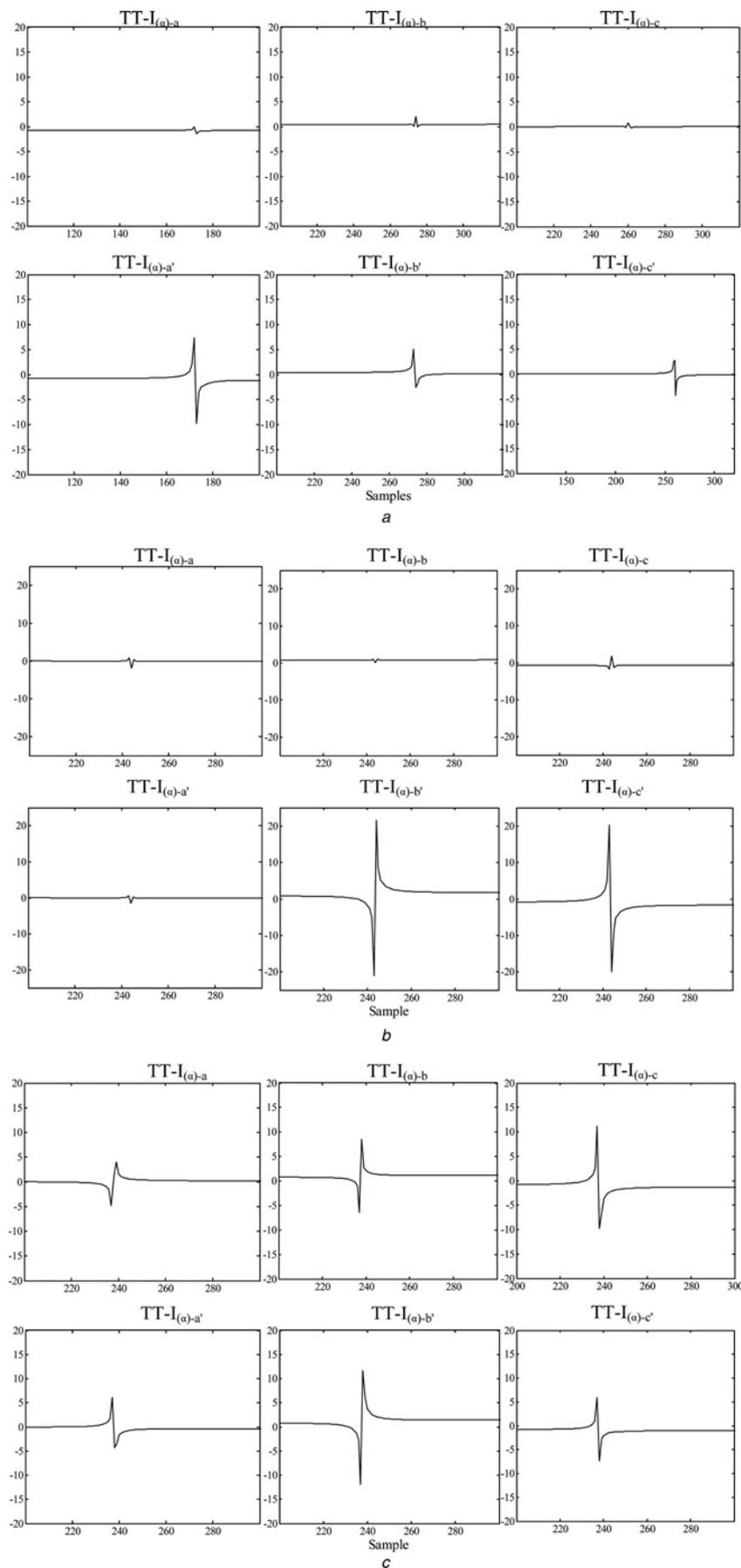**Fig. 9** *Double-circuit three-terminal transmission line configuration*

Fig. 10 *TT-transform of current signals of six phase currents at terminal R*

a Phase-a' to ground fault
b Phase-b' to phase-ć fault
c Phase-c to phase-b' fault

It should be noted that choosing the sampling frequency is a trade-off between being satisfied with the obtained accuracy and the availability of hardware that the software can be implemented on.

4.7 Effect of untransposed lines

Assuming the three-terminal transmission line in Fig. 2 as untransposed lines, different conditions have been simulated while the proposed method has been applied. Table 3 has shown the results of these simulations, where it can be seen that the proposed method is not affected and the accuracy is still acceptable.

4.8 Double-circuit case study

The proposed fault location method has been extended to double-circuit lines, without any modification in the algorithm except that the currents from the phases of the two circuits should be applied to the algorithm. Thus, the modal transformation is done through the following relations instead of (5) and (6)

$$\left[I_{0\alpha\beta0'\alpha'\beta'} \right]_a = \left[T'_{Cl} \right] \cdot \left[I_{abc\ a'b'c'} \right] \quad (11)$$

where (for phases a and a' as the pivots)

$$T'_{Cl} = \begin{bmatrix} T_{Cl} & 0 \\ 0 & T_{Cl} \end{bmatrix} \quad (12)$$

For the network containing this type of line as shown in Fig. 9 (with the same system parameters, given in the appendix), the TT-transform of the modes of six phase currents, at terminal R, in three different fault conditions; that is, phase-to-ground fault and phase-to-phase inter-circuit fault and also crossover fault between the two circuits have been illustrated in Fig. 10. It can be seen that, in all three cases, the faulted phases can be readily revealed according to their peaks, which are larger than the sound phases. This fact rules not only on the phases involved in inter-circuit faults but also on those involved in crossover faults.

Table 4 has shown the results of the proposed fault location algorithm for this line configuration in different fault locations, resistances and inception angles as well as different fault types. It is shown that the proposed algorithm is immune from the fault location (even on tap point), fault resistance and fault type and the error of the estimated fault location is within the acceptable range, even for double-circuit three-terminal lines.

4.9 External fault and lightning contributions

The performance of the proposed fault location method under external faults and lightning are shown in Table 5. In these simulations, external faults are located behind all three terminals, one by one. As it can be seen, the proposed method has good responses under external faults. Moreover, if the lightning strikes hit the line at different locations the proposed algorithm estimates the location with the error of 0.41%.

4.10 Other parameters

The effects of synchronisation error and pre-fault power flow condition on the accuracy of the proposed method are discussed in this subsection.

It is well known that GPS provides a very accurate synchronising system with an error less than 1 μs. Thus, by using 100 kHz as the sampling frequency, the proposed method is not much affected by synchronisation error and even if the maximum possible error is taken in to account, there is only one sample displacement in assigning time of arrivals. Thus, the fault location error does not exceed ± 0.59%.

Investigating the performance of the proposed method for different pre-fault power flow conditions has shown that there is no substantial change in the accuracy of the fault location and the error remains under 0.7%.

Table 4 Estimation error (in %) for different fault types, fault resistances and fault locations in double-circuit line

Fault type	Fault inception angle	Fault resistance, Ω	Actual fault location, km															
			10	20	30	40	50	60	70	75	80	90	100	110	120	130	140	Tap point
a–g	30°	1	0.18	0	0.12	0.41	0.35	0.18	0	0.06	0.41	0.06	0.24	0.18	0.29	0.41	0.06	0.13
a–g	30°	17	0.18	0	0.12	0.41	0.35	0.18	0	0.06	0.41	0.06	0.24	0.18	0.29	0.41	0.06	0.13
a–g	30°	50	0.18	0	0.12	0.41	0.35	0.18	0	0.06	0.41	0.06	0.24	0.18	0.29	0.41	0.06	0.13
a–g	30°	100	0.18	0.29	0.12	0.41	0.35	0.18	0	0.06	0.41	0.06	0.24	0.18	0.29	0.41	0.06	0.13
a–g	0°	30	0.47	0.29	0.12	0.53	0.06	0.12	0.29	0.24	0.18	0.24	0.06	0.12	0.29	0.18	0.35	0.13
b–c	30°	30	0.18	0	0.12	0.41	0.35	0.18	0.29	0.06	0.41	0.06	0.24	0.18	0.29	0.41	0.06	0.13
b–c–g	30°	30	0.18	0	0.12	0.41	0.35	0.18	0	0.06	0.41	0.06	0.24	0.18	0.29	0.41	0.06	0.13
a–b–c	30°	30	0.18	0.29	0.12	0.41	0.64	0.18	0	0.06	0.12	0.06	0.24	0.18	0.29	0.12	0.06	0.13
a–b–c–g	30°	30	0.18	0	0.12	0.41	0.64	0.18	0	0.06	0.41	0.06	0.24	0.18	0.29	0.41	0.06	0.13
b'–c	30°	30	0.18	0.29	0.12	0.06	0.06	0.18	0.29	0.06	0.12	0.06	0.06	0.12	0.29	0.18	0.06	0.13

Table 5 Results upon external fault and lightning

Event	External faults			Lightning		
actual fault location	30 km from R	30 km from S	30 km from T	40 km from R	70 km from R	130 km from R
FL response	external	external	external	39.85	70	131.02

Table 6 Comparing capabilities and extent of the proposed method with the published methods

Algorithm	Evrenosoglu and Abur [3]	Da Silva et al. [5]	Da Silva et al. [6]	Ibe and Cory [2]	Proposed method
maximum error, %	0.324	1	1	2.05	0.71
average error, %	0.103	0.34	NR	1.05	0.163
terminals involved	1	3-S	NR	1	3-S
sampling frequency, kHz	333	240	240	NR	100
effect of fault resistance	R	R	NR	NR	R
effect of fault inception angles	NR	R	NR	R	R
effect of fault location	NR	R	NR	R	R
effect of fault type	NR	R	NR	R	R
effect of faulted section	NR	R	NR	R	R
fault on tap point	NR	NR	NR	NR	R

NR: not reported; S: synchronised data; R: reported

5 Comparing the proposed method with the existing methods

The existent fault location methods based on travelling waves initiated by faults, either have employed wavelet transformation [3–6] or have processed the waves, directly [2].

Not intending to give a quantitative and or precise comparison between those methods and the proposed method, but only to give a qualitative comparison based on the extent of investigations, the sampling frequency used and the accuracy as claimed, the comparative results are summarised in Table 6. It can be seen that the only one which has reported its results for all conditions (except for faults on tap points) has employed higher sampling frequency and has claimed lower accuracy.

6 Conclusions

This paper has presented a new fault location method, employing TT-transform, for three-terminal lines. The TT-transform is used to extract high-frequency components generated by fault for fault detection and determination of arrival time of waves at the line terminals. These arrival time instants are then employed to find the faulted section and ultimately the fault location. Based on a comprehensive study, the results have shown that the proposed fault location method has very accurate performance in both single- and double-circuit lines under different conditions of fault resistance, fault type, fault inception angle, fault location (even on tap point), faulted section and pre-fault power flow. The results have shown that the estimation error of the proposed method is under 0.71% for all conditions.

7 References

1 Saha, M.M., Izykowski, J., Rosolowski, E.: 'Fault location on power networks', (Springer, 2010, 1st edn.)
2 Ibe, A.O., Cory, B.J., 'A travelling wave-based fault locator for two- and three-terminal networks', *IEEE Trans. Power Deliv.*, 1986, vol. 1 (2), pp. 283–288
3 Evrenosoglu, C.Y., Abur, A.: 'Travelling wave based fault location for teed circuits', *IEEE Trans. Power Syst.*, 1986, **PWRD-1**, (2), pp. 1115–1121
4 Spoor, D., Zhu, J.G.: 'Improved single-ended travelling – wave fault location algorithm' *IEEE Trans. Power Deliv.*, 2006, **21**, (3), pp. 1714–1720
5 Da Silva, M., Oleskovicz, M., Coury, D.V.: 'A hybrid fault locator for three-terminal lines based on wavelet transforms', *Electr. Power Syst. Res.*, 2008, **78**, (11), pp. 1980–1988
6 Da Silva, M., Coury, D.V., Oleskovicz, M., Segatto, E.C.: 'Combined solution for fault location in three terminal lines based on wavelet transforms', *IET Gener. Transm. Distrib.*, 2010, **4**, (1), pp. 94–103
7 Chiradeja, P., Pothisarn, C.: 'Identification of the fault location for three-terminal transmission lines using discrete wavelet transforms'. Transmission and Distribution Conference and Exposition: Asia and Pacific, Seoul, 2009, pp. 1–4
8 Mardiana, R., Motairy, H.A., Su, C.Q., 'Ground fault location on a transmission line using high-frequency transient voltages', *IEEE Trans. Power Deliv.*, 2011, **26**, (2), pp. 1298–1299
9 Zhang, D.J., Wu, Q.H., Zhang, J.F., Nuttall, K.I.: 'Accurate fault location based on transients extraction using mathematical morphology', *Electron. Lett.*, 2004, **38**, (24), pp. 1583–1585
10 Styvaktakis, E., Bollen, M.H.J., Gu, I.Y.H.: 'A fault location technique using high frequency fault clearing transients', *IEEE Power Eng. Rev.*, 1999, **19**, (5), pp. 58–60
11 Simon, C., Schimmel, M., Danobeitia, J.J.: 'On the TT-transform and its diagonal elements', *IEEE Trans. Signal Process.*, 2008, **56**, (11), pp. 5709–5713
12 Pinnegar, C.R., Mansinha, L.: 'A method of time–time analysis: the TT-transform', *Digit. Signal Process.*, 2003, **13**, pp. 588–603

8 Appendix

The parameters of the test system:

System voltage: 230 kV, System frequency: 50 Hz

$$E_R = 1\angle 20^\circ, \quad E_S = 1\angle 0^\circ, \quad E_T = 1\angle 10^\circ$$

$$l_{RP} = 150 \text{ km}, \quad l_{SP} = 100 \text{ km}, \quad l_{TP} = 80 \text{ km}$$

$$Z_{R1} = 0.091 + j2.598\ \Omega, \quad Z_{R0} = 0.878 + j4.515\ \Omega$$

$$Z_{S1} = 0.091 + j2.598\ \Omega, \quad Z_{S0} = 0.878 + j4.515\ \Omega$$

$$Z_{T1} = 0.628 + j17.989\ \Omega, \quad Z_{T0} = 2.862 + j14.724\ \Omega$$

$$v = 294\,117.6 \text{ km/s}$$